Generation of tunable, high-order Laguerre-Gaussian petal-like modes from a mid-infrared optical vortex parametric oscillator

Yuxia Zhou,[a,b] Xining Yang,[b] Jianqiang Ye,[b] Yuanyuan Ma,[c]* Ying Wan,[d] Jianxiang Wen,[e] Taximaiti Yusufu[b]*

[a]School of Chemistry and Chemical Engineering, Xinjiang Normal University, Urumqi, Xinjiang, China, 830054
[b]Xinjiang Key Laboratory for Luminescence Minerals and Optical Functional Materials, School of Physics and Electronic Engineering, Xinjiang Normal University, Urumqi, Xinjiang, China, 830054
[c]Graduate School of Engineering, Chiba University, Chiba, Japan, 263-8522
[d]Jiangsu Key Laboratory for Optoelectronic Detection of Atmosphere and Ocean, School of Physics and Optoelectronic Engineering, Nanjing University of Information Science & Technology, Nanjing, China, 210044
[e]Key Lab of Specialty Fiber Optics and Optical Access Networks, School of Communication and Information Engineering, Shanghai University, Shanghai, China, 200444

Abstract. High-order Laguerre-Gaussian (LG) petal-like beams have become a topic of significant interest due to their potential application in next generation optical trapping, quantum optics, and materials processing technologies. In this work we demonstrate the generation of high-order LG beams with petal-like spatial profiles and tunable orbital angular momentum (OAM) in the mid-infrared wavelength region. These beams are generated using idler-resonant optical parametric oscillation (OPO) in a $KTiOAsO_4$ (KTA) crystal. By adjusting the length of the resonant cavity, the OAM of the mid-infrared idler field can be tuned and we demonstrate tuning in the range $0 \sim \pm10$. When using a maximum pump energy of 20.2 mJ, the maximum output energy of high-order modes $LG_{0,\pm5}$, $LG_{0,\pm8}$ and $LG_{0,\pm10}$ were 0.8 mJ, 0.53 mJ and 0.46 mJ respectively. The means by which high-order LG modes with petal-like spatial profiles and tunable OAM were generated from the OPO is theoretically modelled by examining the spatial overlap efficiency of the beam waists of the pump and resonant idler fields within the center of KTA crystal. The methodology presented in this work offers a simple and flexible method to wavelength convert laser emission and generate high-order LG modes.

Keywords: high-order LG petal-like modes, optical parametric oscillator, nonlinear optics, $KTiOAsO_4$, optical vortices.

*Address all correspondence to Taximaiti Yusufu, taxmamat_84@sina.com; Yuanyuan Ma, mayuanyuan612@gmail.com

1 Introduction

Optical vortex laser beams possess a phase singularity and a helical wavefront which twists in the beam's direction of propagation. Every photon of a vortex beam carries orbital angular momentum (OAM) of ℓh, which can be expressed as a phase factor $\exp(i\ell\varphi)$ (where φ is an azimuthal angle).[1-3] The unique characteristics of these beams have enabled new techniques in fields including optical tweezing,[4,5] optical manipulation,[6,7] optical communication,[8,9] nano/microfabrication of helical structured materials[10] and spectroscopy.[11,12] Laguerre-Gaussian (LG) modes are eigen solutions of the Helmholtz equation under cylindrical symmetry, which can

be directly generated from a laser cavity. LG modes are examples of vortex beams. High-order LG modes which have spatial profiles with petal-like features across their azimuth are an important subset of LG modes. These modes have garnered significant attention for use in manipulation of micro-particles,[13,14] super-resolution imaging,[15] and quantum communication.[16] As such, significant research effort has focused on developing methods whereby high-order LG modes with petal-like spatial profiles can be selectively generated from a laser system.

One approach for generation of these types of LG modes is the coherent superposition of two optical vortex modes with opposite azimuthal order.[17] These modes can be generated directly within a laser cavity by controlling the gain/loss of specific cavity modes using intracavity phase modulating elements[18-20] and mode-selection approaches.[21,22] High-order LG modes with petal-like spatial profiles can also be generated by pumping a laser cavity with a ring-shaped pump beam which is slightly offset from the axis of the laser cavity. This method selectively promotes mode overlap between LG modes and the ring-shaped pump beam.[23,24] Another approach is to make use of defect spots and patterns within the laser cavity to force the oscillation of high-order LG modes.[25] More recently, researchers have used spherical aberration from a spherical lens to generate ultra-high-order LG beams with ℓ order beyond 300 from an end-pump Nd: YVO_4 laser at 1064 nm; this is the highest-order LG mode with a petal-like spatial profile demonstrated from an experimental laser system.[26,27]

Non-linear optical processes such as stimulated Raman scattering can be used to induce the generation of high-order LG modes.[28,29] It should be noted that there have been rather few reports of high-order LG mode generation in the mid-infrared wavelength region. The capacity to generate such modes in this wavelength range would be significant and have potential utility in next generation optical trapping, quantum optics, and materials processing applications.

Optical parametric oscillation (OPO) is a non-linear process which has proven effective for the generation of optical vortex beams in the near-infrared and mid-infrared wavelength ranges.[30-35] There have however, been few reports concerning the generation of high-order LG petal-like modes in the mid-infrared wavelength range using OPOs. Recently, our group has demonstrated the generation of an off-axis vortex beam with non-integer OAM states from an OPO with a half-spherical cavity, resulting from the coherent superposition of Gaussian and vortex modes inside the cavity.[36]

In this paper, we report the first demonstration (to the best of our knowledge) of the generation of OAM-tunable, high-order LG petal-like modes in the mid-infrared region from an idler-resonant KTA-OPO pumped by a nanosecond optical vortex source (ℓ_p =1~3). This cavity enables the selective generation of high-order $LG_{0,\pm\ell}$ (ℓ=0~10) petal-like modes (with controllable OAM) in the mid-infrared region by adjusting the cavity length. Our experimental work is supported by theoretical modelling which analyzes the spatial overlap efficiency of the beam waists of the pump and resonant idler fields within the center of the KTA crystal.

2   Experimental methods

The experimental setup of the mid-infrared OPO generating high-order LG modes with petal-like spatial profiles is shown in Fig. 1. A flash lamp pumped Q-switched Nd:YAG laser which had a Gaussian output beam, pulse width of 25 ns, pulse repetition frequency of 50 Hz and emission wavelength of 1064 nm was used as the pump source. A half-wave plate, thin film polarizer and Faraday rotator (isolator) was used to control the power of the pump beam and prevent back reflection into the laser cavity. Multiple spiral phase plates (SPPs) (azimuthally divided into 16 parts with an $n\pi/8$ phase shift) were combined to convert the pump beam into an optical vortex beam. By using different arrangements of SPP, the topological charge ℓ of the pump beam could

be changed from 1-3. A half-wave plate was used to adjust the polarization of the pump vortex beam so as to optimize phase-matching within the OPO. Using a lens with focal length f=750 mm, the pump vortex beam was focused to a spot with a waist of 380 μm (ℓ_p=1), 474 μm (ℓ_p=2) and 510 μm (ℓ_p=3) at the center of the KTA crystal.
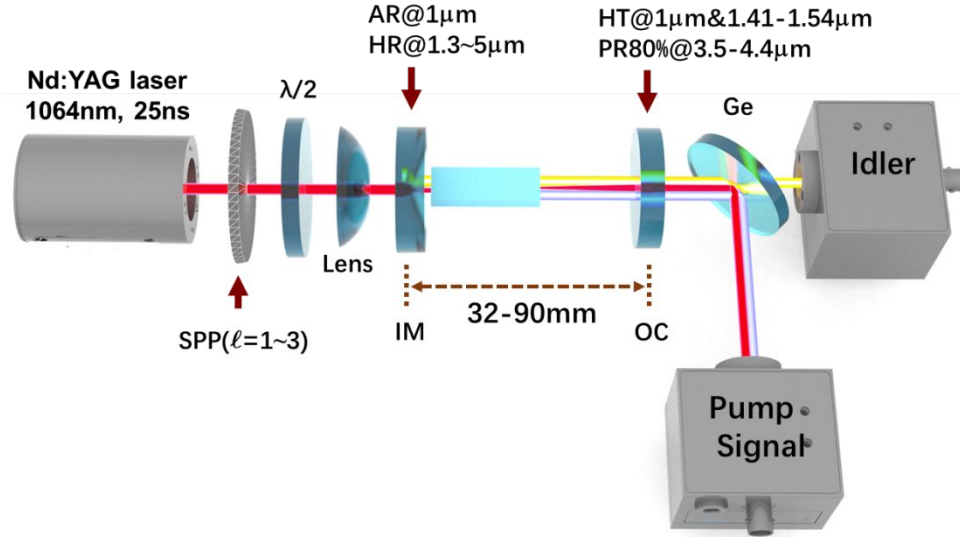

Fig. 1 Schematic showing the layout of the system used to generate mid-infrared high-order LG modes from a vortex-pumped optical parametric oscillator.

The idler-resonant KTA-OPO had a hemispherical cavity comprising a concave input mirror (IM) with radius of curvature R=100 mm and a plane output coupler (OC). The IM was antireflection coated for 1.064 μm and high-reflection coated for 1.3-5 μm (R=99%); the OC was coated partially-reflecting (R≈80%) for the idler beam and high-transmitting for the pump and signal beams. A type II non-critically phase-matched KTA crystal (*x*-cut, θ= 90°, φ= 0°) with dimensions of 5× 5 × 30 mm³ was used in the OPO. Both sides of the crystal were antireflection coated for the pump, signal and idler fields in order to minimize loss. The OC was mounted on a one-dimensional translation stage, the geometrical length of the cavity (*L*) was varied in the range

of 32-90 mm by moving the OC along the optical axis. The IM and KTA crystal were then fixed. A Ge filter was used to separate the idler output from the undepleted pump and signal outputs.

3   Results and Discussion

In these experiments we first generated high-order $LG_{0,\pm\ell}$ modes with tunable topological charge by varying the resonant cavity length of the OPO. The spatial intensity profile of the pump beam was recorded using a CCD camera and that of the signal and idler beams using a pyroelectric camera (Spiricon Pyrocam III, spatial resolution 75 μm). When the OPO was pumped with a first order optical vortex $\ell_p = 1$ (spatial profile shown in Fig. 2(a)), the signal field was generated with a similar spatial profile as shown in Fig. 2(c). The OAM characteristics of the pump and signal beams were examined using the tilted lens method.[37] The spatial profile of the pump and signal beams after being focused through the tilted lens are shown in Figs. 2(b) and 2(d), respectively. In both cases, the presence of two lobes at the focal plane confirm the order of both the pump and the signal vortex beams to be $\ell=1$. This result is in agreement with conservation of OAM within an OPO wherein the OAM of the pump beam is transferred to the non-resonant signal beam. Generally, the idler beam should exhibit a Gaussian spatial profile, however, this was not always observed in this work. The spatial profile of the idler beam (as recorded using the pyroelectric camera) for a range of resonant cavity lengths are shown in Figs. $2(e_1) - 2(e_6)$. It can be seen that the spatial intensity profile of idler beam changes with cavity length. Here, the order of the idler beam LG mode (and the number of petals in the spatial profile) can be increased by decreasing the length of the resonant cavity. The theoretically modelled spatial intensity profiles of the generated LG modes are shown for comparison in Figs. $2(f_1) - 2(f_6)$. There have been a number of publications reporting the generation of similar mode shapes directly from a laser cavity.[38,39] These mode shapes can arise from the coherent superposition of LG modes with opposite azimuthal order

oscillating within the laser cavity (such modes can freely oscillate within the cavity if no additional mode-control elements are used).
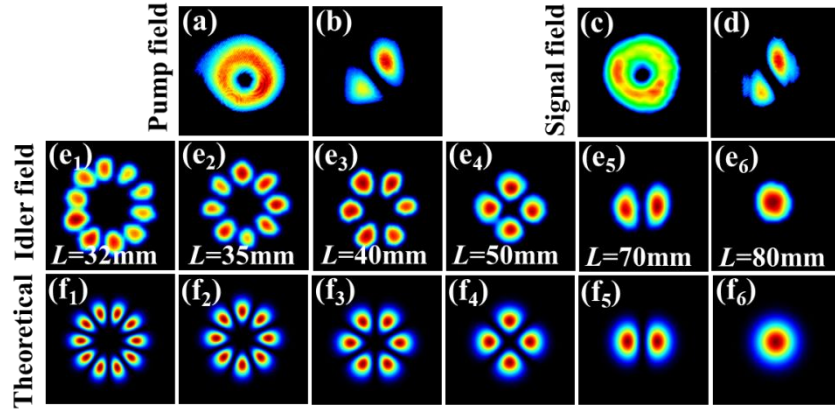

Fig. 2 Images showing the spatial intensity distribution of (a) the free space and (b) focused (through a tilted lens) pump vortex beam with OAM=1. Images of the spatial intensity distribution of (c) the free space and (d) focused (through a tilted lens) signal beam. Images (e_1-e_6) show the experimentally obtained spatial profiles of the idler beam for a range of cavity lengths; and images (f_1-f_6) show the corresponding theoretically modelled spatial intensity profiles of these beams.

To further investigate the generation of high-order LG petal-like modes, the idler-resonant OPO was pumped using vortex beams with ℓ_p=2 and 3. When the OPO was pumped with a second order vortex beam (ℓ=2) (free space and tilted lens focused spatial intensity profiles shown in Figs. 3(a) and 3(b), respectively), the generated signal beam was observed to have a doughnut-shaped intensity profile and carried an OAM of ℓ=2. The free space and tilted lens focused spatial intensity profiles of the generated signal beam are shown in Figs. 3(c) and 3(d) respectively. The results show that the signal field takes on the same OAM characteristics as the pump field; this characteristic was observed for all examined lengths of resonant cavity. The idler fields were generated in the form of high-order LG petal-like modes and its OAM could be tuned from 0 to ±8 by varying the length of the resonant cavity. The experimentally obtained spatial intensity

profiles of the generated idler beams are shown in Figs. 3 (e_1-e_9) for a range of resonant cavity lengths.

When the OPO was pumped using an optical vortex of order ℓ_p, of 3 (free space and tilted lens focused spatial intensity profiles shown in Figs. 3(g) and 3(h), respectively), the generated signal beam was observed to have a doughnut-shaped intensity profile and carried an OAM of $\ell=3$; this characteristic was observed for all investigated lengths of the resonant cavity. The free space and tilted lens focused spatial intensity profiles of the generated signal beam are shown in Figs. 3(i) and 3(j), respectively. By adjusting the length of the resonant cavity, the idler field could be generated in the form of high-order LG petal-like modes and its OAM could be tuned from 0 to ± 10. The experimentally obtained spatial intensity profiles of the generated idler fields are shown in Figs. 3 (k_1-k_{11}) for a range of resonant cavity lengths.
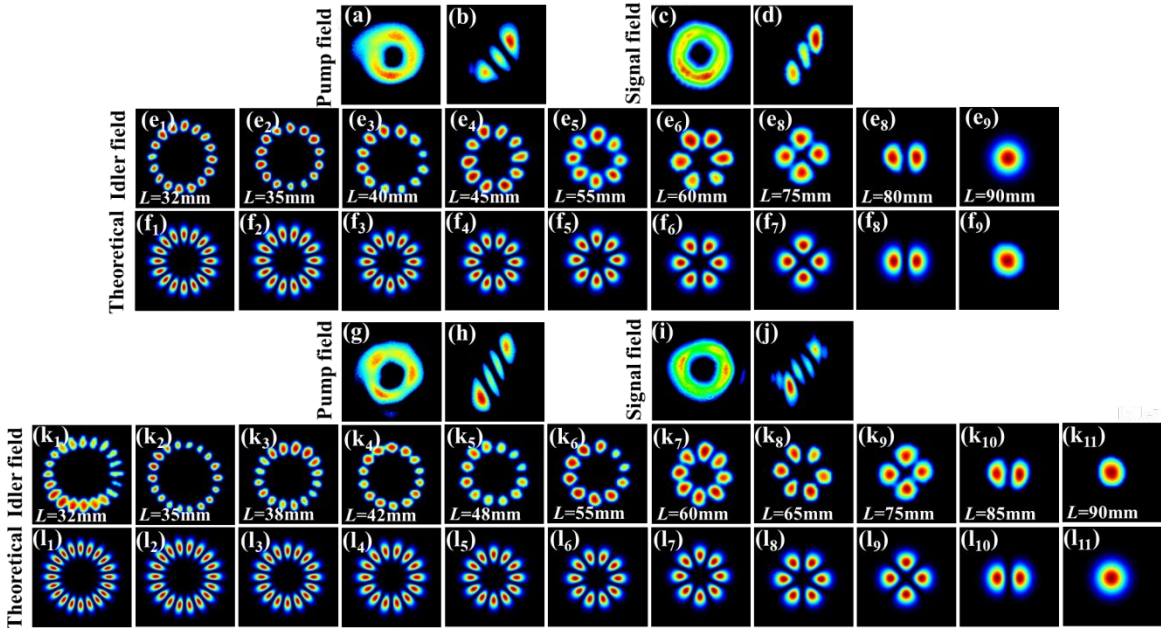

Fig. 3 A collection of images showing the spatial intensity profiles of modes generated when the OPO is pumped with vortex modes of order $\ell=2$ and 3. (a) and (b) show the free space and focused (through a tilted lens) pump vortex beam with $\ell=2$, respectively; (c) and (d) show the corresponding profiles of the generated signal field. (e_1) – (e_9) show the free space spatial intensity profiles of the generated idler field, for a range of resonant cavity lengths and (f_1) – (f_9) are

images of the corresponding theoretically modelled mode profiles. (g) and (h) show the free space and focused (through a tilted lens) pump vortex beam with ℓ=3, respectively; (i) and (j) show the corresponding profiles of the generated signal field. (k_1) – (k_{11}) show the free space spatial intensity profiles of the generated idler field, for a range of resonant cavity lengths and (l_1) – (l_{11}) are images of the corresponding theoretically modelled mode profiles.

The above results show that high-order LG modes with petal-like spatial profiles and tunable OAM can be generated directly from an idler-resonant KTA-OPO by adjusting the length of its resonant cavity. In fact, the handedness ($\pm\ell$) of LG mode with the same intensity profile cannot be well distinguished in the laser cavity, thereby resulting in the generation of petal-like modes formed of the coherent superposition of annular $LG_{0,+\ell}$ and $LG_{0,-\ell}$ modes. To better understand how these high-order LG modes were produced from this system, we performed theoretical modelling wherein we examined the spatial overlap of the pump field with the cavity modes of the idler field within the resonant cavity of the OPO and the KTA crystal. The spatial overlap efficiency η of the pump intensity $I_p(r,z)$ and the cavity mode intensity $I_c(r,z)$ was modelled using the following equation,

$$\eta = \iint I_p(r,z)I_c(r,z)drdz \ (1)$$

The normalized intensity distribution of an $LG_{0,\ell}$ mode can be expressed as,[40]

$$I(r,\varphi,z) = \frac{2}{\pi w_0^2 d l!}\left[\frac{2r^2}{w_0^2}\right]^{|l|}[L_p^{|l|}\left(\frac{2r^2}{w_0^2}\right)]^2 \ exp\left(\frac{-2r^2}{w_0^2}\right)\begin{Bmatrix}sinl\varphi\\cosl\varphi\end{Bmatrix}^2 \ (2)$$

Where $L_p^{|l|}(\cdot)$ is the generalized Laguerre polynomial, p and ℓ are the radial and azimuthal indices, respectively. d is the length of the gain medium, and w_0 is the cavity mode size, which is assumed to be constant in the laser crystal (along the axis of the laser).

If we consider a focused donut-shaped vortex pump beam, we can define the beam radius r_{outer} as the radius of a circle which contains 86.5% of the total energy of the beam, and the ring radius

r_{inner} as the radius of circle which contains 13.5% the total energy. The equation determining the spatial overlap efficiency can then be modified to,[41]

$$\eta = \sum_{n=0}^{l} \frac{1}{(l-n)!} \left[\left(\frac{2r_{inner}^2}{w_0^2} \right)^{l-n} \exp\left(-\frac{2r_{inner}^2}{w_0^2} \right) - \left(\frac{2r_{outer}^2}{w_0^2} \right)^{l-n} \exp\left(-\frac{2r_{outer}^2}{w_0^2} \right) \right] \quad (3)$$

Where the waist (w_0) of the fundamental cavity mode of a plano-concave linear cavity can be determined using,[42]

$$w_0 = \sqrt{\frac{L_{eff}\lambda}{\pi}} \left[\frac{g_1 g_2 (1-g_1 g_2)}{(g_1 + g_2 - 2g_1 g_2)^2} \right]^{1/4} \quad (4)$$

Here, $L_{eff}=L-(n_r-1)d/n_r$ is the effective resonator length, λ is the wavelength of the lasing mode, n_r is the refractive index of the gain medium, $g_i = (1-L_{eff})/R_i$ is the g-factor of the resonator, and R is the radius of curvature of the cavity mirrors. The values of r_{inner} and r_{outer} were determined directly from our experiment. Here, the values of r_{inner} and r_{outer} for pump vortex beams with ℓ_p=1 − 3 were 35.6 μm and 330 μm; 92.1 μm and 410 μm; 132.8 μm and 440 μm, respectively. Using these values along with the above equations, we theoretically modelled the spatial overlap efficiency (η) as a function of the resonant cavity mode order (ℓ). These results are plotted in Fig. 4 for pump vortex beams with ℓ_p=1 − 3.
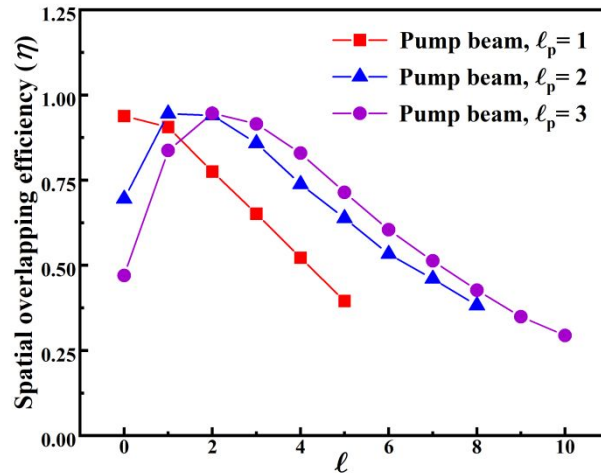
Fig. 4 Plots of the theoretically modelled spatial overlap efficiency as a function of resonant cavity mode order (ℓ) for pump vortex beams with topological charge ℓ_p of $1 - 3$.

Fig. 4 shows the calculated spatial overlap efficiency η between the vortex pump mode and high-order LG modes within the resonant cavity of the OPO at various cavity lengths (32~90 mm). When pumping with a vortex beam with order ℓ_p=1, the spatial overlap efficiency (red square) decreases monotonically as ℓ increases. When pumping with vortices of order, ℓ_p=2 and 3, the spatial overlap efficiency first increases and then decreases as the value of ℓ increases. The high-order LG mode which is generated from the resonant cavity is a function of both the intracavity loss of that mode and the spatial overlap of the pump field with that mode. Both of these factors are a function of the length of the resonant cavity. The output energies of the signal and idler beams were measured as a function of the pump energy when pumping with vortex beams of order ℓ_p=1 $- 3$ and for a range of resonant cavity lengths. These plots are shown in Fig.5.
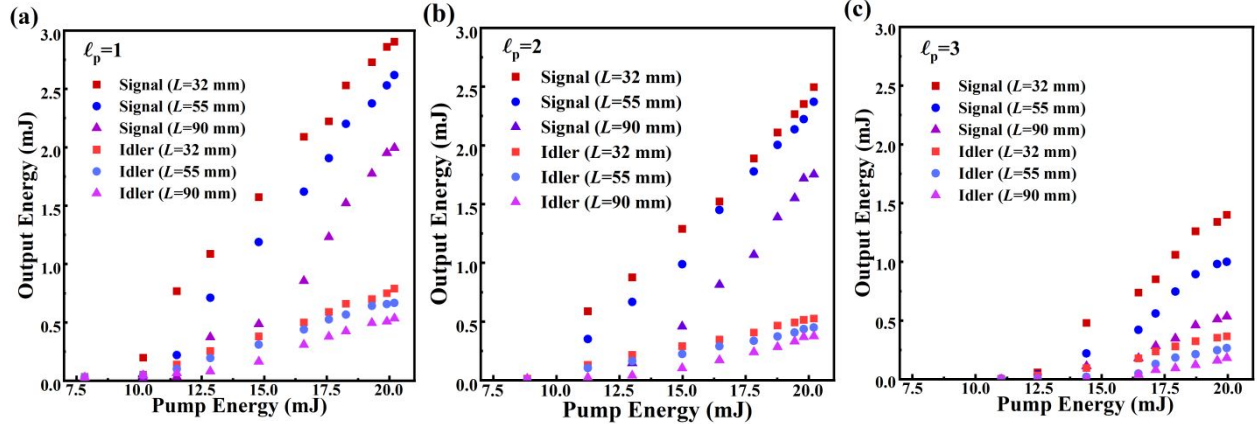

Fig. 5 Plots showing the output energies of the signal and high-order LG mode idler fields as a function of incident pump energy and for different resonant cavity lengths. (a) Shows results using a pump vortex beam with ℓ_p=1; (b) shows results using a pump vortex beam with ℓ_p=2; and (c) shows results using a pump vortex beam with ℓ_p=3.

The plot of Fig. 5(a) shows that when using a pump field with ℓ_p=1 and an energy of 20.2 mJ, for cavity lengths of L=32 mm, 55 mm, and 90 mm, the maximum output energies of the signal and idler fields were 2.9 mJ, 2.6 mJ, 2.1 mJ, and 0.8 mJ, 0.67 mJ, 0.54 mJ, respectively. The

corresponding slope efficiencies were 23.5%, 28.9%, 22.9% and 6.4%, 7.4%, 6.2%, respectively. Fig. 5 (b) shows that the maximum output energies of the signal and idler fields when using a pump field with ℓ_p=2 for cavity lengths of L=32 mm, 55 mm and 90 mm were 2.5 mJ, 2.3 mJ, 1.8 mJ, and 0.53 mJ, 0.45 mJ, 0.38 mJ, respectively. Fig. 5 (c) shows that the maximum output energies of the signal and idler fields when using a pump field with ℓ_p=3 for cavity lengths of L=32 mm, 55 mm and 90 mm were 1.4 mJ, 1 mJ, 0.54 mJ, and 0.37 mJ, 0.27 mJ, 0.18 mJ, respectively. The corresponding to slope efficiencies were 18.7%, 12.8 % 7.2%, and 4.9%, 3.6%, 2.4%, respectively. It should be noted that the oscillation threshold of high-order petal-like modes increases, as the extending of cavity length from 32 mm to 90 mm, which is due to the severe cavity loss. The measured oscillation threshold of OPO pumped by the optical vortex with order of, ℓ_p=1~3, were ranged within 7.7-10.2 mJ, 7.9-11.2 mJ and 11.2-14.4 mJ, respectively. From these results, it is clear that pumping with the lowest order vortex mode yields the highest signal and idler output energies for a given pump energy and resonant cavity length.

The spectra of the signal and idler outputs (measured to be 1535 nm and 3468 nm, respectively) were recorded using a scanning monochromator (Spectra Pro HRS-500, 300 lines/mm, aperture size 30 μm, spectral resolution of 0.3-0.4 nm in the wavelength range of 1000-5000 nm) and are plotted in Fig. 6. The spectral bandwidths of the signal and idler outputs were measured to be $\Delta\lambda_s$~ 0.32 nm (ca. 1.36 cm^{-1}) and $\Delta\lambda_i$~ 0.67 nm (ca. 0.56 cm^{-1})
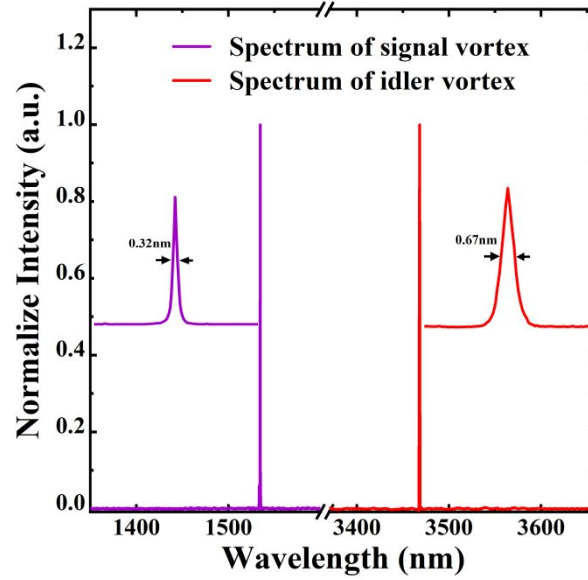
Fig. 6 Plots of the output signal (1535 nm) and idler (3468 nm) field spectra; insets are zoomed spectra highlighting the spectral bandwidth of each field.

4 Conclusions

In conclusion, we have demonstrated the generation of high-order $LG_{0,\pm\ell}$ mode idler field vortex beams with ℓ tunable from 0 to ±10 using an idler-resonant KTA-OPO. The order of the output idler beam could be varied by adjusting the length of the resonant cavity and by changing the order of the vortex pump beam. A theoretical investigation of the spatial overlap efficiency of the pump vortex and resonant idler beams was undertaken in order to glean insight into the mechanism by which these high-order LG modes were generated. When pumped with vortex beams with $\ell = 1$, 2 and 3, due to the increasing of spatial overlap efficiency, the highest order idler beams that could be generated from the system were $LG_{0,\pm5}$, $LG_{0,\pm8}$, $LG_{0,\pm10}$, respectively. This work demonstrates the relative ease by which high-order LG laser modes in the mid-infrared wavelength range can be generated directly from an OPO system. We anticipate that such laser beams will have utility for applications in precise spatial measurements, optical trapping and tweezing, and free space optical/quantum communications.

References

1. L. Allen, M. W. Beijersbergen, R. J. C. Spreeuw, and J. P. Woerdman, "Orbital angular momentum of light and the transformation of Laguerre-Gaussian laser modes," *Phys. Rev. A* **45**(11), 8185–8189 (1992).[doi:10.1103/PhysRevA.45.8185]

2. M. S. Soskin, and M. V. Vasnetsov, "Singular Optics," *Prog. Opt* **42**(4), 219–276 (2001). [doi:10.1016/s0079-6638(01)80018-4]

3. A. M. Yao, and M. J. Padgett, "Orbital angular momentum: origins, behavior and applications," *Adv. Opt. Photonics* **3**(2), 161-204 (2011). [doi:10.1364/AOP.3.000161]

4. T. Omatsu, K. Miyamoto, K. Toyoda, R. Morita, and K Dholakia, "Twisted Materials: A New Twist for Materials Science: The Formation of Chiral Structures Using the Angular Momentum of Light," *Adv. Opt. Materials* **7**(14), 1801672 (2019). [doi:10.1002/adom.201801672]

5. J. Chen, C. H. Wan, and Q. W. Zhan, "Engineering photonic angular momentum with structured light: a review," *Adv. Photonics*, **3**(6), 064001-064001. (2021). [doi: 10.1117/1.AP.3.6.064001]

6. D. G. Grier, "A revolution in optical manipulation," *Nature* **424**(6950), 810-816 (2003). [doi:10.1038/nature01935]

7. Y. J. Shen, X. J. Wang, Z. W. Xie, C. J. Min, X. Fu, Q. Liu, M. L. Gong, and X. C. Yuan, "Optical vortices 30 years on: OAM manipulation from topological charge to multiple singularities," *Light: Sci. Appl* **8**(1), 1-29 (2019). [doi:10.1038/s41377-019-0194-2]

8. J. Wang, "Advances in communications using optical vortices," *Photonics Res* **4**(5), B14-B28 (2016). [doi:10.1364/prj.4.000b14]

9. J. Wang, "Advances in communications using optical vortices," Photonics Res 4(5), B14-B28 (2016). [doi:10.1364/prj.4.000b14]

10. J. Ni, C. Wang, C. Zhang, Y. Hu, L. Yang, Z. Lao, B. Xu, J. Li, D. Wu, and J. Chu, "Three-dimensional chiral microstructures fabricated by structured optical vortices in isotropic material," *Light Sci. Appl.* 6(7), e17011 (2017). [doi:10.1038/lsa.2017.11]

11. M. Vainio, and L. Halonen, "Mid-infrared optical parametric oscillators and frequency combs for molecular spectroscopy," *Phys. Chem. Chem. Phys* **18**(6), 4266–4294. (2016). [doi: 10.1039/c5cp07052j]

12. S. Bretschneider, C. Eggeling, and S. W. Hell, "Breaking the diffraction barrier in fluorescence microscopy by optical shelving," *Phys. Rev. Lett* **98**(21), 218130 (2007). [doi:10.1103/physrevlett.98.218103]

13. K. T. Gahagan, and G. A. Swartzlander, "Optical vortex trapping of particles," *Opt. Lett* **21**(11), 827-829 (1996).[doi.org/10.1364/OL.21.000827]

14. Z. Zhu, Y. Q. Zhang, S. Zhang, J. L. Adam. Aurèle, C. J. Min, H. P. Urbach, and X. C. Yuan, "Nonlinear optical trapping effect with reverse saturable absorption," *Adv. Photonics*, **5**(4), 046006-046006. (2023). [doi: 10.1117/1.AP.5.4.046006]

15. S. Bretschneider, C. Eggeling, and S. W. Hell, "Breaking the diffraction barrier in fluorescence microscopy by optical shelving," *Phys. Rev. Lett* **98**(21), 218130 (2007). [doi:10.1103/physrevlett.98.218103]

16. J. C. Fang, J. P. Li, A. Kong, Y. P. Xie, C. X. Lin, Z. W. Xie, T. Li, and X. C. Yuan, "Optical orbital angular momentum multiplexing communication via inversely-designed multiphase plane light conversion," *Photonics Res* **10**(9), 2015-2023 (2022). [doi:10.1364/PRJ.458474]

17. D. Naidoo, K. Aït-Ameur, M. Brunel and A. Forbes, "Intra-cavity generation of superpositions of Laguerre–Gaussian beams," *Appl. Phys. B* **106**, 683-690 (2012). [doi:10.1007/s00340-011-4775-x]

18. N. R. Heckenberg, R. McDuff, C. P. Smith, and A. G. White, "Generation of optical phase singularities by computer generated holograms," *Opt. Lett* **17**(3), 221–223 (1992). [doi:10.1364/ol.17.000221]

19. G.A. Turnbull, D.A. Robertson, G.M. Smith, L. Allen, and M.J. Padgett, "The generation of free-space Laguerre-Gaussian modes at millimetre-wave frequencies by use of a spiral phase plate," *Opt. Commun* **127**(4-6), 183-188 (1996). [doi:10.1016/0030-4018(96)00070-3]

20. R. J. Li, Y. Ren, T. Liu, C. Wang, Z. L. Liu, J. Zhao, R. S. Sun, and Z. Y. Wang. "Generating large topological charge Laguerre–Gaussian beam based on 4K phase-only spatial light modulator," *Chin. Opt. Lett* **20**(12), 120501 (2022). [doi:10.3788/col202220.120501]

21. W. Koechner, Solid-state laser engineering, 6th ed. (Semantic Scholar 2006), pp.211–231.

22. A. Ito, Y. Kozawa, and S. Sato, "Generation of hollow scalar and vector beams using a spot-defect mirror," *JOSA. A* **27**(9), 2072-2077 (2010). [doi: 10.1364/josaa.27.002072]

23. Y. F. Chen, and Y. P. Lan, "Dynamics of the Laguerre Gaussian TEM$_{0,\ell}$* mode in a solid-state laser," *Phys Rev A* **63**(6), 063807 (2001). [doi:10.1103/PhysRevA.63.063807]

24. Y. F. Chen, and Y. P. Lan, "Dynamics of helical-wave emission in a fiber-coupled diode end-pumped solid-state laser," *Appl. Phys. B* **73**(1), 11–4 (2001). [doi: 10.1007/s003400100566]

25. Z. Qiao, G. Q. Xie, Y. H. Wu, P. Yuan, J. G. Ma, L. J. Qian, and D. Y. Fan, "Generating High-Charge Optical Vortices Directly from Laser Up to 288th Order," *Laser Photonics Rev*. **12**(8), 1800019 (2018).

[doi: 10.1002/lpor.201800019]

26. Q. Sheng, A. H. Wang, Y. Ma, S. J. Wang, M. Wang, Z. Shi, J. Liu, S. J. Fu, W. Shi, J. Q. Yao, and T. Omatsu, "Intracavity spherical aberration for selective generation of single-transverse-mode Laguerre-Gaussian output with order up to 95," *PhotoniX.* **3**(1), 4 (2022). [doi: 10.1186/s43074-022-00050-8]

27. Q. Sheng, A. H. Wang, J. N. Geng, S. J. Fu, Y. Ma, W. Shi, J. Q. Yao, T. Omutsu, and D. Spence, "Ultra-High-Order Laguerre-Gaussian Field Generated Directly from a Laser Cavity with Spherical Aberration," *Laser Photonics Rev* **17**(8), 2300369 (2023). [doi: 10.1002/lpor.202300369]

28. A. J. Lee, T. Omatsu, and H. M. Pask, "Direct generation of a first-stokes vortex laser beam from a self-Raman laser," *Opt. Express* **21**(10), 12401–9 (2013). [doi: 10.1364/OE.21.012401]

29. Y. J. Miao, L. Zhang, and J. Dong, "Broadband Petal-Like Raman Laser," *Ann. Phys* **534**(4), 2100476 (2022). [doi: 10.1002/andp.202100476]

30. M. Martinelli, J. A. O. Huguenin, P. Nussenzveig, and A. Z. Khoury, "Orbital angular momentum exchange in an optical parametric oscillator," *Phys. Rev. A* **70**(1), 013812 (2004). [doi:10.1103/physreva.70.013812]

31. T. Yusufu, Y. Tokizane, M. Yamada, K. Miyamoto, and T. Omatsu, "Tunable 2-μm optical vortex parametric oscillator," *Opt. Express* **20**(21), 23666–23675 (2012). [doi:10.1364/oe.20.023666]

32. M. Ababaike, S. T. Wang, P. Aierken, T. Omatsu, and T. Yusufu. "Near and mid-infrared optical vortex parametric oscillator based on KTA," *Sci. Rep* **11**(1), 1-6 (2021). [doi:10.1038/s41598-021-86945-1]

33. A. Aadhi, G. K. Samanta, S. Chaitanya Kumar, and M. Ebrahim-Zadeh, "Controlled switching of orbital angular momentum in an optical parametric oscillator," *Optica* **4**(3), 349–355 (2017). [doi:10.1364/optica.4.000349]

34. A. Abulikemu, S. Yakufu, Y. X. Zhou, and T. Yusufu, "Mid-infrared idler-resonant optical vortex parametric oscillator based on MgO:PPLN," *Opt. Laser Technol* **171**, 110341 (2024). [doi: 10.1016/j.optlastec.2023.110341]

35. D. Jashaner, Y. X. Zhou, and T. Yusufu, "Widely-tunable mid-infrared (2.6–5 μm) picosecond vortex

laser," *Appl. Phys. Express* **15**, 102004 (2022). [doi: 10.35848/1882-0786/ac92c1]

36. Y. X. Zhou, T. Yusufu, Y. Ma, and T. Omatsu, "Generation of tunable, non-integer OAM states from an optical parametric oscillator," *Appl. Phys. Lett* **122**(12), (2023). [doi: 10.1063/5.0141377]

37. P. Vaity, J. Banerji, and R. P. Singh, "Measuring the topological charge of an optical vortex by using a tilted convex lens," *Phys. Lett* **377**(15), 1154-11562013, (2013). [doi: 10.1016/j.physleta.2013.02.030]

38. M. Okida, T. Omatsu, M. Itoh, and T. Yatagai, "Direct generation of high power Laguerre-Gaussian output from a diode-pumped Nd:YVO$_4$ 1.3-μm bounce laser," *Opt. Express* **15**(12), 7616-7622 (2007). [doi:10.1364/OE.15.007616]

39. J. W. Kim, J. I. Mackenzie, J. R. Hayes, and W. A. Clarkson, "High power Er: YAG laser with radially-polarized Laguerre-Gaussian (LG$_{01}$) mode output," *Opt. Express* **19**(15), 14526-14531 (2011). [doi:10.1364/OE.19.014526]

40. R. L. Phillips, and L. C. Andrews, "Spot size and divergence for Laguerre Gaussian beams of any order," *Appl. Opt* **22**(5), 643-644 (1983). [doi:10.1364/ao.22.000643]

41. J. W. Kim, and W. A. Clarkson, "Selective generation of Laguerre–Gaussian (LG0n) mode output in a diode-laser pumped Nd: YAG laser," *Opt. Commun* **296**, 109-112. (2013). [doi:10.1016/j.optcom.2013.01.046]

42. S. Y. Luo, X. G. Yan, Q. Cui, B. Xu, H. Y. Xu, and Z. P. Cai, "Power scaling of blue-diode-pumped Pr:YLF lasers at 523.0, 604.1, 606.9, 639.4, 697.8 and 720.9 nm," *Opt. Commun* **380**, 357-360 (2016). [doi: 10.1016/j.optcom.2016.06.026]

Yuxia Zhou received her MS degree in optics from Xinjiang Normal University, China, in 2023. She is currently a PhD student at the Chemistry and Chemical Engineering and Xinjiang Key Laboratory for Luminescence Minerals and Optical Functional Materials, Xinjiang Normal University, China. Her research focuses on analysis chemistry, nonlinear optics, optical vortices, optical parametric oscillator and amplifier.

Xining Yang received her PhD in Testing and measurement technology and instruments from the Harbin University of science and technology, China, in 2020. She is currently professor at the Xinjiang Key Laboratory for Luminescence Minerals and Optical Functional Materials, Xinjiang Normal University, China. Her research focuses on Solid laser.

Jianqiang Ye received his BS degree in applied physics from Jiangsu University of science and technology, China, in 2022. He is currently a MS student at the Xinjiang Key Laboratory for Luminescence Minerals and Optical Functional Materials, Xinjiang Normal University, China. His research focuses on optical vortices, optical parametric oscillator and amplifier.

Yuanyuan Ma received her PhD in Optical Engineering from the Graduate School of Advanced Integration Science, Chiba University, Chiba, Japan, in 2020. She is currently a Postdoctoral Research Fellow in the Graduate School of Engineering at Chiba University. Her research area focuses on structured-light beam generation and solid-state Raman lasers.

Ying Wan received her PhD in Communication and Information Systems from the Shanghai University, China, in 2022. She is currently a lecturer at Nanjing University of Information and Technology, China. Her research interests focus on optical fiber, nonlinear frequency conversion.

Jianxiang Wen received his PhD in Communication and Information Systems from Shanghai University, Shanghai, in 2011. Currently, he is an associate professor at Shanghai University. His current research interests include special optical fiber structure design, research, and preparation.

Taximaiti Yusufu received his PhD in Optical Engineering from the Graduate School of Advanced Integration Science, Chiba University, Japan, in 2014. He worked as a postdoctoral research associate in the Laser Laboratory at the Chiba University, Japan, from 2014 to 2015. He is currently a professor at the Xinjiang Key Laboratory for Luminescence Minerals and Optical Functional Materials, Xinjiang Normal University, China. He is Vice Director of the School of

Physics and Electronic Engineering, Xinjiang Normal University, China. He is the author of more than 50 journal papers. His current research interests include optical vortices, OAM, structured light, nonlinear optics, optical parametric oscillator and amplifier.

Caption List

Fig. 1 Schematic showing the layout of the system used to generate mid-infrared high-order LG modes from a vortex-pumped optical parametric oscillator.

Fig. 2 Images showing the spatial intensity distribution of (a) the free space and (b) focused (through a tilted lens) pump vortex beam with OAM=1. Images of the spatial intensity distribution of (c) the free space and (d) focused (through a tilted lens) signal beam. Images (e_1-e_6) show the experimentally obtained spatial profiles of the idler beam for a range of cavity lengths; and images (f_1-f_6) show the corresponding theoretically modelled spatial intensity profiles of these beams.

Fig. 3 A collection of images showing the spatial intensity profiles of modes generated when the OPO is pumped with vortex modes of order ℓ=2 and 3. (a) and (b) show the free space and focused (through a tilted lens) pump vortex beam with ℓ=2, respectively; (c) and (d) show the corresponding profiles of the generated signal field. (e_1) – (e_9) show the free space spatial intensity profiles of the generated idler field, for a range of resonant cavity lengths and (f_1)- (f_9) are images of the corresponding theoretically modelled mode profiles. (g) and (h) show the free space and focused (through a tilted lens) pump vortex beam with ℓ=3, respectively; (i) and (j) show the corresponding profiles of the generated signal field. (k_1) – (k_{11}) show the free space spatial intensity profiles of the generated idler field, for a range of resonant cavity lengths and (l_1)- (l_{11}) are images of the corresponding theoretically modelled mode profiles.

Fig. 4 Plots of the theoretically modelled spatial overlap efficiency as a function of resonant cavity mode order (ℓ) for pump vortex beams with topological charge ℓ_p of $1 - 3$.

Fig. 5 Plots showing the output energies of the signal and high-order LG mode idler fields as a function of incident pump energy and for different resonant cavity lengths. (a) Shows results using a pump vortex beam with ℓ_p=1; (b) shows results using a pump vortex beam with ℓ_p=2; and (c) shows results using a pump vortex beam with ℓ_p=3.

Fig. 6 Plots of the output signal (1535 nm) and idler (3468 nm) field spectra; inset are zoomed spectra highlighting the spectral bandwidth of each field.